# Wavelet and Lipschitz exponent based damage identification method for beams using mode shapes

**Abstract**

This paper presents a damage identification method for beam-type structures based on the wavelet analysis. The damage location is predicted by a Damage Locating Index (DLI) based on a combined identification of local maxima from the scalograms of mode shapes. A new Damage Severity Index (DSI) based on the Lipschitz exponent is formulated such that it is not dependent from the damage locations, boundary conditions, and mode order, as long as a high enough number of measuring points is considered. This study focuses on its application using relatively few measurement points and on the consistency of the DSI. Results from a beam with double-notch damage are analyzed. The results show that the method is applicable with a sparse measurement grid and the DSI Reference values from a static analysis can be referred for damage evaluation using modal displacements. The practical limits of the method are also discussed.

*Keywords:* beams, multiple damage, mode shapes, wavelet transform, sparse measurements

## 1. Introduction

Damage identification methods solve the problem successively through detection, location, and quantification. Detection and location can be done by analyzing the abnormality in between the post-damage structural response and the reference structural response, either from a static, dynamic, or modal analysis. Quantification can be solved by comparing a damage state with reference values that can be obtained using numerical or analytical models. Nevertheless, there is always a difference between a model and a real structure, which can not be ascertained unless it is identified using measurements. In this paper, existing formulation of a Damage Locating Index (DLI) and a Damage Severity Index (DSI) [1] based on the Continuous Wavelet Transform (CWT) and Lipschitz exponent are redefined and extended for the application of damage identification from the experimental mode shapes of a damaged beam. The paper explores the applicability of the identification method from three perspectives: (1) the robustness and limitations of the proposed DLI on an oscillating signal (mode shapes) obtained from a sparse measuring grid; (2) the application of the DSI to modal displacements and its independence from boundary conditions and damage location; and (3) the potential use of the same DSI Reference values from either a static or any modal response for the evaluation of the damage.

A structural damage is defined as an alteration of the material or geometry properties over a local region, which results in a sudden change in the slope of the displacement field. A simple example is a notch on a beam. Although this type of damage is rarely seen in practice, it is commonly used in academic research due to its simple geometric form (easy to be artificially introduced and geometrically defined) and direct quantification relationship between notch depth and damage severity. In this study, the notch is considered always in the open state so that the structural response can reflect the effect of damage. At the location of damage, the induced abnormality in the displacement field (both static deflections and mode shapes) will result in a local peak value of wavelet coefficients [2–7]. Common methods to determine the location of these local peaks include the use of a 2D color map [2, 3, 8] or the use of combined wavelet coefficients through different scales [9, 10]. Apart from the exploitation of wavelet scales in damage detection, the mode order is also utilized in this paper for the determination of DLI. This paper also addresses the issues on the prediction of the damage location due to the oscillation of the wavelet function and the consequent shifts of wavelet local peaks caused by the use of a symmetric wavelet function.

In the application of CWT for damage detection, the number of samples of the discrete space signal directly affects the damage location accuracy. Kumar and Singh [8] compares the use of 100, 200, and 1000 measurement points for the application of CWT for damage detection and indicates that the accuracy of the results is affected significantly. Hence, numerical studies on this topic consider usually a high number of measurement points and the experimental studies are conducted with measuring systems that can obtain a dense measurement grid, such as laser scanning [7, 11] and photogrammetry measuring system [1, 8, 12–14]. In Table 1, the number of samples in some relevant research studies are listed. Although a high density of measurements can be obtained experimentally, the associated experimental techniques are limited to small scale structures. For large scale structures, traditional sensors, such as accelerometers and strain gauges are more common in practice. The number of measurements of the conventional sensors is, however, much lower. A total of 33 measurement points of the dynamic response of the tested beam in this study are acquired by using piezoelectric accelerometers.

Efforts to estimate the damage severity have led to different proposals of damage indices based on the wavelet coefficients using static deflections [1, 9, 15]. Static testing is simple and efficient. However, it is not always practicable for certain types of structures. Damage indices based on modal analysis, can be developed using the Lipschitz exponent-wavelet characteristic [10, 16, 17]. Nevertheless, the damage indices proposed in the cited literature are dependent on the damage location, mode order, and boundary conditions. In contrast, the method proposed in a previous study by the authors [1] normalizes the wavelet local peak coefficients to the curvature at its location, which leads to a DSI that is independent from the damage location, mode order, and the boundary conditions. It is a major advantage that the damage method does not require the identification of actual behavior of the boundary conditions in practice applications. However, when using a limited number of measurement points, the accuracy of the estimation of modal curvatures is reduced. Interpo-

Table 1: Number of samples in the CWT application on Damage Identification.

| Research | Analysis type | Displ. type | Beam Length | Number of samples |
|---|---|---|---|---|
| Cao et al. [3] | Numerical | Mode shape | 500 mm | 500 |
| Ghanbari Mardasi et al. [6] | Numerical | Static | 1000 mm | 1001 |
| | Experimental | Static | 26.5 mm | 1080 |
| Deng et al. [7] | Numerical | Mode Shape | 500 mm | 1001 |
| | Experimental | Mode Shape | 500 mm | 499 |
| Kumar and Singh [8] | Numerical | Mode Shape | 1000 mm | 1000 |
| | Experimental | Static | 1000 mm | 1000 |
| Nigam and Singh [13] | Numerical | Mode Shape | 1000 mm | 4000 |
| | Experimental | Static | 1000 mm | $\approx 2400$ |
| Andreaus et al. [9] | Experimental | Static | 280 mm | 312 |

lation is one alternative way to artificially increase the number of measuring points [18–20]. However, when using data with experimental noise, on one hand, interpolation might introduce extra unwanted disturbance in the data, which can lead to false-positive errors in damage detection. On the other hand, results are highly sensitive to noise, especially with a sparse measurement grid. Therefore, in this study, a polynomial curve fitting is proposed to reduce the experimental noise so no interpolation is adopted, minimizing artificial intervene to the measurement data. One should note that when using mode shapes, a mode is obviously non-sensitive to a damage that is located at its nodes (zero modal amplitude locations). Cross-reference of potential damage locations among different modes can resolve this issue.

The paper is outlined as follows: first the damage identification method is presented together with a brief review of the CWT background. The development of the DLI and DSI are illustrated for the estimation of damage location and severity, respectively. A numerical example is used to show the performance of the indices with both dense and sparse measurements. Next, experimental results of a simply-supported beam with two notches are presented to verify the applicability of the method with real experimental noise pollution and a sparse measuring grid. Finally, the outputs of the research are discussed and conclusions are drawn.

## 2. Damage identification method

The proposed damage identification method is developed based on the theory presented in References [1, 21] for static deflections. In this section, the theory is briefly reviewed and extended to the application with mode shapes. Hereinafter, the undamaged state of the structure is denoted by the Reference State (State R) and the damaged state of the structure is denoted by the Damaged State (State D).

*2.1. Damage induced effect in the displacement field*

For a beam structure which is well restrained and subjected to some external static forces that generate a pure bending displacement field $u_{\mathrm{R}}(x)$ and internal bending moment distribution $m_{\mathrm{R}}(x)$, being $x$ the longitudinal coordinate along the beam, the presence of a concentrated damage will result in a change in $u_{\mathrm{R}}(x)$. Denote the post-damage displacement field by $u_{\mathrm{D}}(x)$ and let the damage location be $x_0$. The stiffness change at $x_0$ reduces the bearing capacity of the cross-section, thereby modifying the moment distribution and displacement field along the beam. It can be demonstrated [22, 23] that the damage induced variation of the displacement field, $\Delta u(x)$ ($\Delta u(x) = u_{\mathrm{D}}(x) - u_{\mathrm{R}}(x)$), is equivalent to the response of the damaged beam subjected to a pair of self-equilibrated bending moments that equals $m_{\mathrm{R}}(x_0)$, applied at $x_0$. This state of the beam is named the Incremental State (State I) and the corresponding response of the structure is denoted by $u_{\mathrm{I}}(x)$, where $u_{\mathrm{I}}(x)$ is equal to $\Delta u(x)$.

The bending bending moment of the damaged beam is denoted by $m_{\mathrm{D}}(x)$. The difference between the external bending moment applied in the State I at the damage location ($m_{\mathrm{R}}(x_0)$) and $m_{\mathrm{D}}(x_0)$ corresponds to the moment transmitted to both sides of the damage in the State I, which are represented by $m_{\mathrm{I}}^{-}(x_0)$ and $m_{\mathrm{I}}^{+}(x_0)$ (for left and the right side of the damage, respectively): $m_{\mathrm{I}}^{-}(x_0) = m_{\mathrm{I}}^{+}(x_0) = m_{\mathrm{R}}(x_0) - m_{\mathrm{D}}(x_0)$. Therefore, the bending moment in the State I at the damage location ($m_{\mathrm{I}}(x_0)$) is equal to $m_{\mathrm{D}}(x_0)$. A detailed explanation of this decomposition scheme can be found in [22, 23].

Similarly, in modal analysis, we denote the undamaged and damaged $j$th mode shapes by $\phi_{\mathrm{R},j}(x)$ and $\phi_{\mathrm{D},j}(x)$, and their corresponding modal bending moments by $m_{\mathrm{R},j}(x)$ and $m_{\mathrm{D},j}(x)$, respectively. The Incremental State of the $j$th mode is described as the beam subjected to a pair of self-equilibrated harmonic bending moments, of an amplitude equal to the modal bending moment $m_{\mathrm{R},j}(x_0)$, acting at the damage location with a frequency equal to the $j$th natural frequency. The resulting operational deflection $\phi_{\mathrm{I},j}(x)$ is equal to the mode shape difference ($\phi_{\mathrm{D},j}(x) - \phi_{\mathrm{R},j}(x)$), and the resulting operational bending moment at the damage location ($m_{\mathrm{I},j}(x_0)$) is equal to the modal bending moment at that location in State D ($m_{\mathrm{D},j}(x_0)$), as illustrated in Figure 1.

From a practical perspective, it must be noted that, since the damage characterization is based on the change of the modal response of the beam, both undamaged and damaged modal data must be collected experimentally, as it is illustrated in Section 4 with an experimental case study.

*2.2. Wavelet transform and damage indices*

A wavelet function is a zero-mean function that oscillates within a certain span. The Continuous Wavelet Transform (CWT) of a signal is the convolution of a wavelet function and the signal. The span of the wavelet function can be shifted by the translation parameter $v$ and stretched or shrinked by the scale parameter $s$ in the CWT:

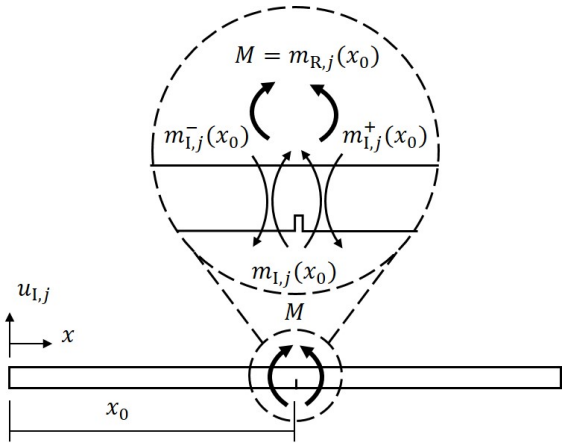


Figure 1: The Incremental State of the beam.

$$Wf(v,s) = \frac{1}{\sqrt{s}} \int_{-\infty}^{+\infty} f(x)\psi^* \left( \frac{x-v}{s} \right) \mathrm{d}x \tag{1}$$

where $f(x)$ is the signal, $\psi^*(x)$ is the complex conjugate of the wavelet function, and $Wf$ is the wavelet coefficient of $f(x)$ at position $v$ for a certain scale $s$. An important feature of the wavelet function is its number of vanishing moments. This number defines the highest order of a polynomial for which the wavelet transform would provide null values. If a function $f(x)$ can be approximated by a polynomial of order $n$, $p^n(x)$, and the wavelet function has $n+1$ vanishing moments, then the CWT of the function would be the same as applying the CWT to the residual $\varepsilon(x)$ between the original function $f(x)$ and the polynomial approximate (Eqs. (2) and (3)):

$$f(x) = p^n(x) + \varepsilon(x) \tag{2}$$

$$Wf(v,s) = W\varepsilon(v,s) \tag{3}$$

In this application, the CWT is applied to each mode shape difference $\phi_{\mathrm{I},j}$ ($f(x) = \phi_{\mathrm{I},j}$ in Eq. (1), (2), and (3)). Different wavelet functions exhibit different characteristics in detecting singularity in signals. More details of wavelet functions and their application for damage detection can be found in References [24–26]. Based on a previous study [1], the Gaussian wavelet with 4 vanishing moments ('Gaus4') is used in this work. When applying CWT with finite length signals, the wavelet coefficients tends to be infinite at the two ends of the signal. To adjust this issue, the finite signal is usually padded at both ends. Several different padding methods can be found in References [27, 28]. In this study, the asymmetric padding is used.

When using a wavelet function which results in local extreme values at the discontinuity of the signal in the space-scale domain, the line connecting these local extreme values across the

scales is known as the "wavelet ridge". In the application of damage detection, the damage locations can be identified using the "wavelet ridge". By utilizing this property, the proposed DLI is based on the count of the appearance of the wavelet coefficient local extreme values at each position:

$$\mathrm{DLI}_{i,j} = \sum_{k=1}^{R} \mathrm{index}_{i,j,k} \tag{4}$$

$$\mathrm{index}_{i,j,k} = \begin{cases} 1 & \text{if } Wf_j(x_i, s_k) \text{ is local maximum;} \\ -1 & \text{if } Wf_j(x_i, s_k) \text{ is local minimum;} \\ 0 & \text{everywhere else.} \end{cases} \tag{5}$$

where $i = 1, 2, \cdots, N$, $j = 1, 2, \cdots, M$, and $k = 1, 2, \cdots, R$, being $N$ be the number of measurement points, $M$ be the number of identified modes, and $R$ be the number of scales used in the wavelet transform. The damage are located at points where the absolute value of DLI is equal to $R$.

For the severity quantification, a different property of the wavelet transform at the identified discontinuity locations is used. At each one of those locations ($x_0$), the wavelet coefficients for each mode $j$ satisfy:

$$|Wf_j(x_0, s)| \leqslant As^{\alpha+1/2}, \quad \text{where} \quad q = 1, 2, \cdots, P \tag{6}$$

where $A$ is a constant and $\alpha$ is the Lipschitz exponent of the signal at $x_0$. Constant $A$ is related to the magnitude of the discontinuity and $\alpha$ is related to the discontinuity order [1, 16, 17, 29]. Dividing both sides of Eq. (6) by the modal bending moment at the damage location in State I (which equals the bending moment in State D at that location as stated before) and taking logarithms one gets:

$$\log_2(Wf'_j(x_0, s)) \leqslant A' + (\alpha + 1/2)\log_2 s \tag{7}$$

$$Wf'_j(x_0, s) = \left| \frac{Wf_j(x_0, s)}{m_{D,j}(x_0)} \right| \quad \text{and} \quad A' = \log_2\left(\frac{A}{|m_{D,j}(x_0)|}\right) \tag{8}$$

being $Wf'_j(x_0, s)$ the normalized wavelet coefficients at $x_0$ and $A'$ is defined as the Damage Severity Index (DSI) for location $x_0$ of mode $j$. If damage is considered as a local physical discontinuity (as represented traditionally by a lumped spring model), the local singularity in the response of the beam is defined just by the damage severity and the bending moment that is acting at the damaged section. Considering $K_r$ as the stiffness of the rotational spring that connects the two undamaged parts of the beam, then $m_{\mathrm{D,j}}(x_0) = K_r \Delta\theta_{I,j}$, being $\Delta\theta$ the rotation discontinuity of the beam (first order derivative of the displacement field).

Based on this assumption, the discontinuity at $x_0$ is proportional to the modal bending moment $m_{\mathrm{D,j}}(x_0)$. Thus, the normalization procedure makes the DSI be only dependent on the damage severity and independent from the damage location. Further details on this issue can be found in [1].

The DSI can be obtained for all the available measurement points along the beam. Then, the damage severity can be estimated at each point by comparing the DSI value with a Reference Map, as explained in the next section.

### *2.3. Reference Map of the Damage Severity Index*

The damage quantification procedure requires the comparison of the obtained DSI on the real beam with reference values of known damage severity levels. The reference values can be obtained numerically from a finite element model of the beam with the same cross-section and material properties (hereinafter referred as the Reference Model) by following the procedure described in the previous section. The numerical response (static or modal displacements and bending moment distributions) is obtained for the undamaged and damaged states at the same locations as the sensors. From the results obtained from the Reference Model, the Reference Map can be plotted by representing the DSI values for different damage severity levels.

The boundary conditions of the Reference Model do not theoretically require to be consistent with the real beam since the effect of the damage is locally analyzed at the damage location. This is a practical advantage because of the uncertainty about the actual behavior of the real boundary conditions. However, a reduced number of measuring points may affect the independence of the DSI with respect to the boundary conditions as well as the damage location. In such situations, the accuracy of the identification procedure can be reduced by this influence on the validity of the Reference Map. All these issues are discussed and analyzed from a numerical illustration in the next section.

## 3. Numerical illustration

A numerical model of a beam with two notches is exemplified to demonstrate the procedure to obtain the proposed DLI, DSI, and Reference Maps. The performance of the identification method with different densities of measurements is also illustrated. A finite element model is used for the simulation of an experimental test with a double damage scenario. A similar model is also used for obtaining the Reference Map for the damage quantification step. First, the results of a dense measuring grid are presented to show the independence of the DSI from the damage locations, boundary conditions, and mode orders. Then, a sparse measuring grid is considered for simulating a practical situation, in which the influence of the number of measuring points, and the limits of the method are discussed.

A finite element model of a beam with rectangular cross-section of dimensions $700(L) \times 80(W) \times 20(H)$ mm (length×width×height) is built with 10-node tetrahedral quadratic solid elements. The beam is made of steel ($7850\,\mathrm{kg/m^3}$ density, 210 GPa Young's Modulus, and 0.3

Poisson ratio). Two notches of 1 mm width and uniform depth throughout the cross-section are included in the model at 170 mm and 470 mm with different depths ($d$) and corresponding relative severity ($\xi = d/H$), as listed in Table 2. The beam is simply-supported and the first 5 bending modes (mass-normalized) are obtained.

Table 2: Damage definition parameters.

| Damage | location (mm) | depth (mm) | severity (%) |
|---|---|---|---|
| D1 | 170 | 10 | 50 |
| D2 | 470 | 5 | 25 |

The mode shapes corresponding to State R, State D and State I are shown in Figure 2. When using the mode shapes for damage detection, a damage may be located at a node for certain modes, which the modes would not be sensitive to that damage. In the presented example, D2 in Mode 3 and D1 in Mode 4 are close to a node, in which the identification of damage will be more sensitive to errors. In addition, it should be noted that, in a multi-damage scenario of different severity, the discontinuity induced by the lower severe damage may not be perceptible in $\phi_{\mathrm{I}}$, which will complicate the damage locating when noise is presented, such as D2 in Mode 2 and Mode 5.

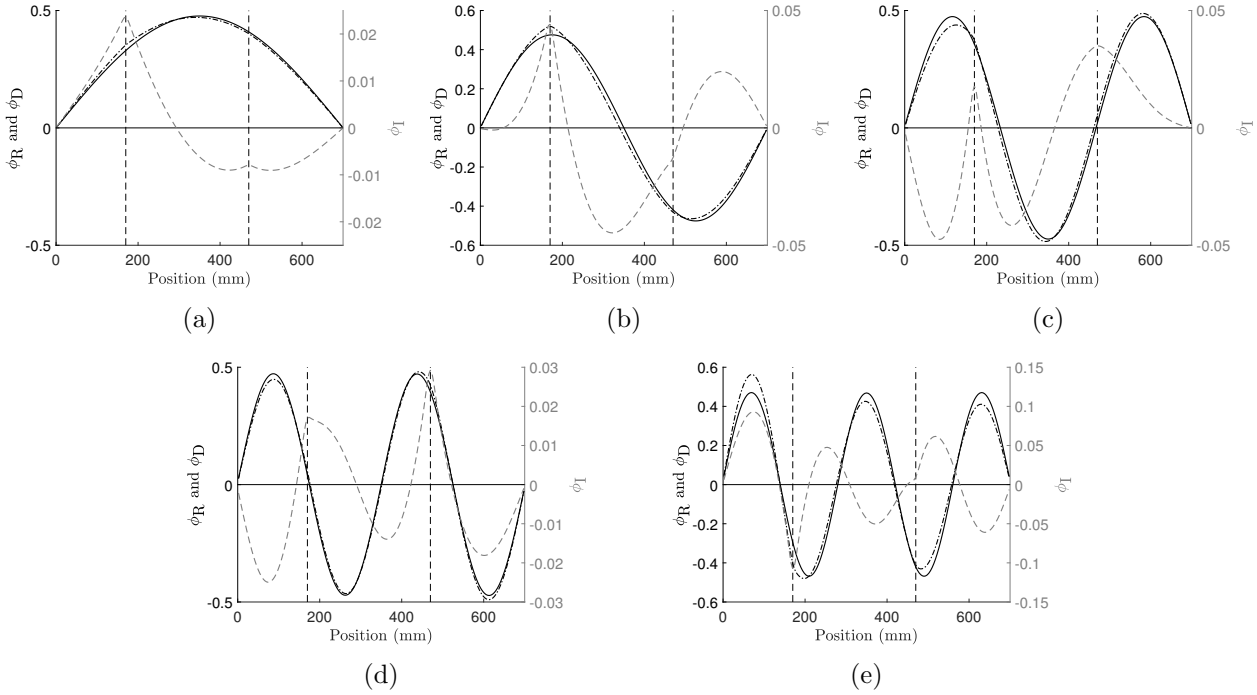


Figure 2: Five reference mode shapes ($\phi_{\mathrm{R}}$, black solid lines), damaged mode shapes ($\phi_{\mathrm{D}}$, black dash-dotted lines), and corresponding incremental mode shapes ($\phi_{\mathrm{I}}$, gray dashed lines) of the example: (a) Mode 1, (b) Mode 2, (c) Mode 3, (d) Mode 4, (e) Mode 5 (the vertical dashed lines mark the damage locations).

Two sets of numerical measurements of different densities are considered. One consists of 176

measurement points with a 4 mm spacing, considered a dense grid example and denoted by Set-4, and the other one consists of 35 measurement points with a 20 mm spacing, considered a sparse grid example and denoted by Set-20.

### *3.1. Dense grid (Set-4)*

In this case, four scales are used for the wavelet transform though a higher number could be considered for that large number of measuring points. Figure 3 shows that the wavelet coefficients affected by the two damage are well separated. The wavelet coefficients at D1 (more severe) are higher than those at D2 (less severe) as shown in all modes except in Mode 4 (Figure 3 (d)), in which D1 is close to a node and consequently its effect is diminished. A similar phenomenon can be observed in Mode 3 for D2 (Figure 3 (c)) due to its proximity to a node. The wavelet coefficients of the less severe damage (D2) are higher than the more severe one (D1). In case that the damage is not distinguishable due to the presence of experimental noise, the detection of such a damage would rely on other modes.

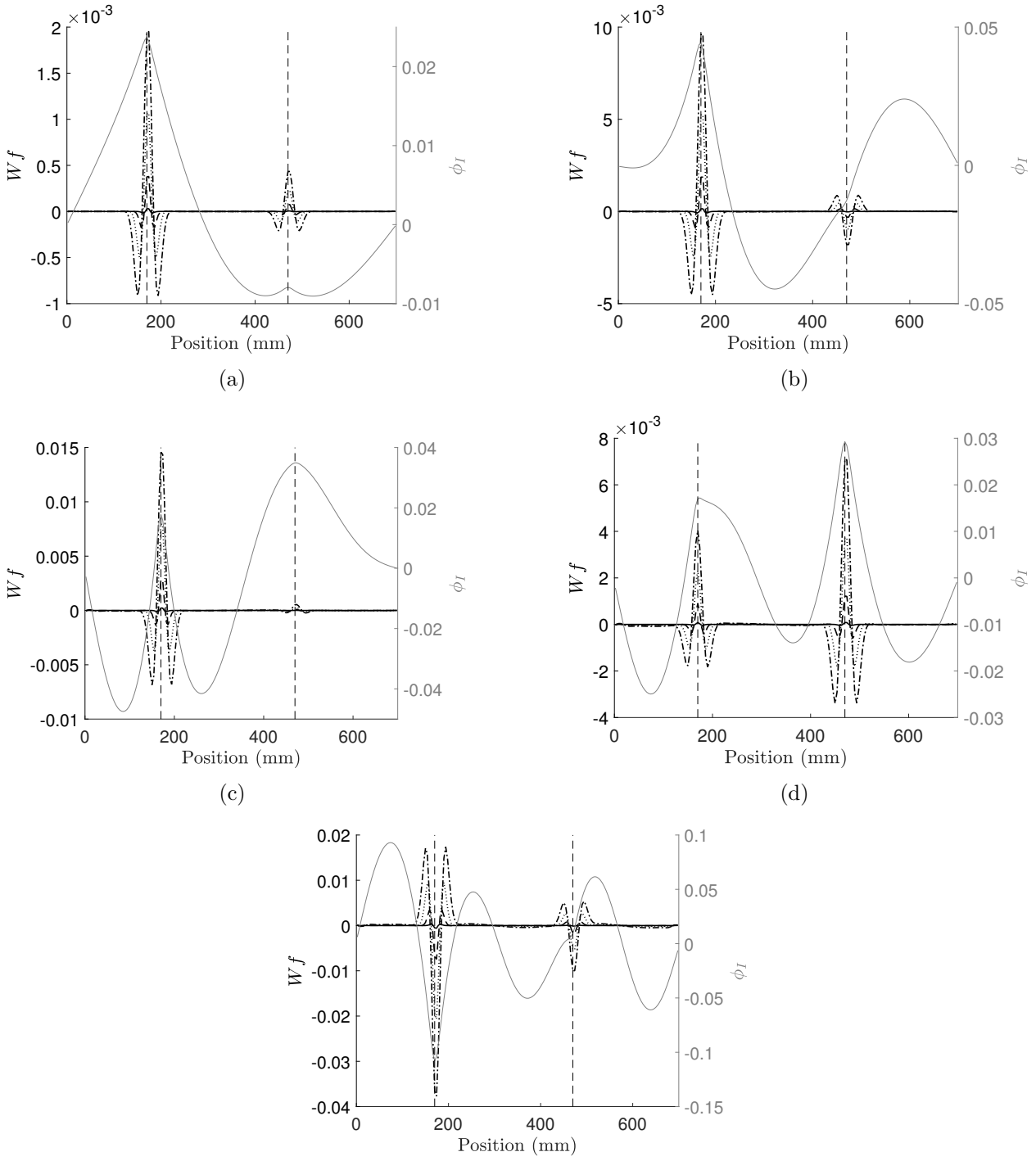


Figure 3: Incremental mode shapes (gray solid lines) and their wavelet coefficients (black lines) of the numerical example of Set-4: (a) Mode 1, (b) Mode 2, (c) Mode 3, (d) Mode 4, (e) Mode 5 (Scale 1: solid lines; Scale 2: dashed lines; Scale 3: dashed-dotted lines; Scale 4: dotted lines; the vertical dashed lines mark the damage locations).

Figure 3 also shows that wavelet coefficients are close to zero when damage is out of the wavelet span. Thus, the corresponding region should be considered undamaged. Figure 4 shows the DLI of each mode of Set-4. It must be noted that, due to the symmetry of Gaus4 wavelet, the local extreme values appear either at the damage locations or at adjacent measurement points, depending on the incremental mode shape. Moreover, because of the oscillatory behavior of the wavelet coefficients, the maximum absolute values of DLI are accompanied with several single unity peaks of a different sign. These additional peaks appear at different locations because of the different spans of the wavelet function for each scale, thereby, dispersing the local extreme values due to the oscillation around the damage. Thus, only locations with an absolute value of DLI of 4 are considered as damage locations (Table 3).

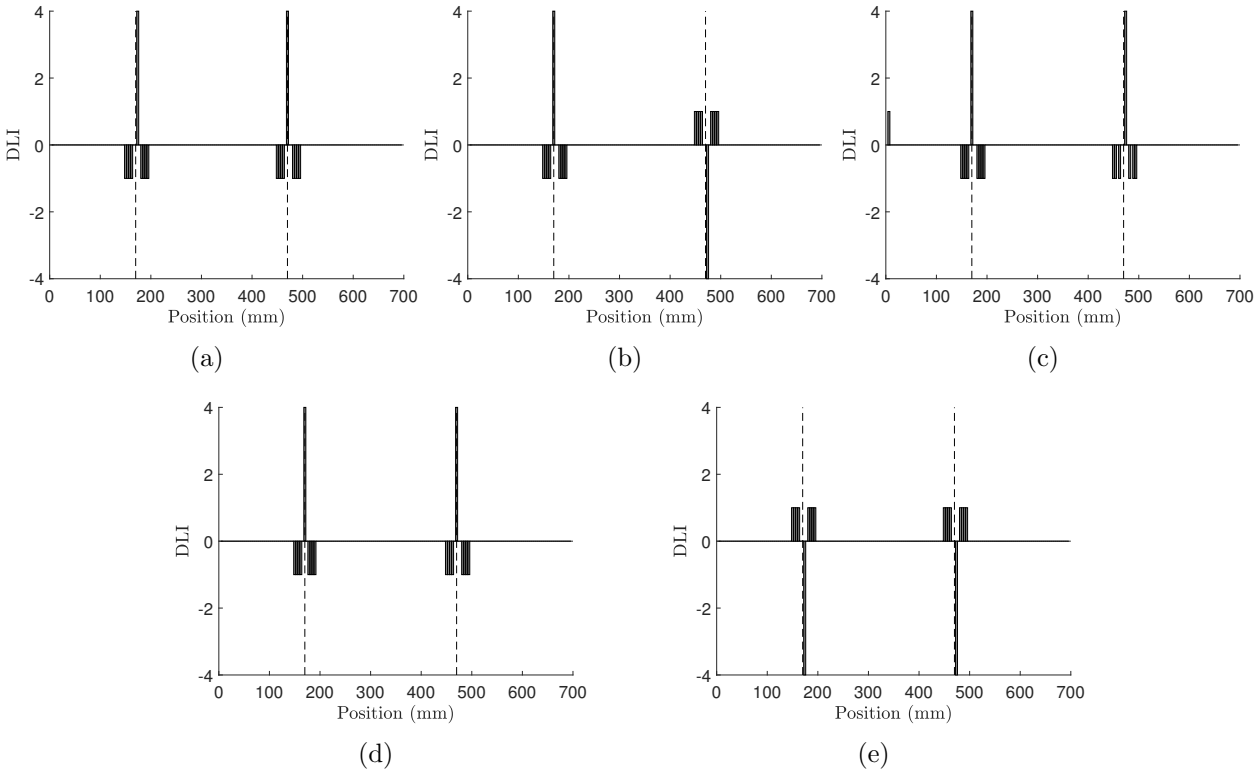


Figure 4: DLI of each mode of the Set-4: (a) Mode 1, (b) Mode 2, (c) Mode 3, (d) Mode 4, (e) Mode 5.

Table 3: Predicted damage locations (mm) of the Set-4 example.

| Damage | Mode 1 | Mode 2 | Mode 3 | Mode 4 | Mode 5 |
|---|---|---|---|---|---|
| D1 | 174 | 170 | 170 | 170 | 174 |
| D2 | 470 | 474 | 474 | 470 | 474 |

Once the damage locations are identified, the quantification process is addressed through the use of the DSI. As presented previously, this process requires the normalization of the

DSI with the values of the bending moment in State D at the damage locations. This can be done by computing the modal curvature through the well-known Strength of Materials relationship under linear elastic behavior for slender beams (shear strain is neglected), i.e., $m_{\mathrm{D}} = EI\mathrm{d}^2\phi_{\mathrm{D}}/\mathrm{d}x^2$, where $E$ is the elastic modulus and $I$ is the inertia of the cross section. For the numerical computation of the curvature, a finite difference scheme can be applied. However, even in noise free conditions, a sudden peak takes place at the damage locations due to the instability of the curvature around a concentrated damage. Despite this instability in the curvature distribution, it mus be noted that, because of equilibrium, the bending moment distribution is a continuous and soft function along the beam. The sudden change in the curvature is accompanied by a sudden change in stiffness, making the bending moment at the damaged section consistent with the values at the adjacent undamaged regions. Thus, the bending moment distribution along the beam, including the damaged sections, can be accurately estimated by neglecting the local peaks in the curvature distribution induced by damage and considering the undamaged beam bending stiffness. For this purpose, a curve fitting process is proposed to estimate the bending moment distribution at the Damaged State.

For the presented numerical results, Figure 5 shows the obtained distributions of the undamaged and damaged bending moments. For the latter, the spline curve fitting is also included. It can be seen that the curve fitting provides a good estimation of the values at the damage locations. For illustration and comparison purposes, Table 4 includes the numeric values of the damaged and undamaged bending moments at the damage locations.

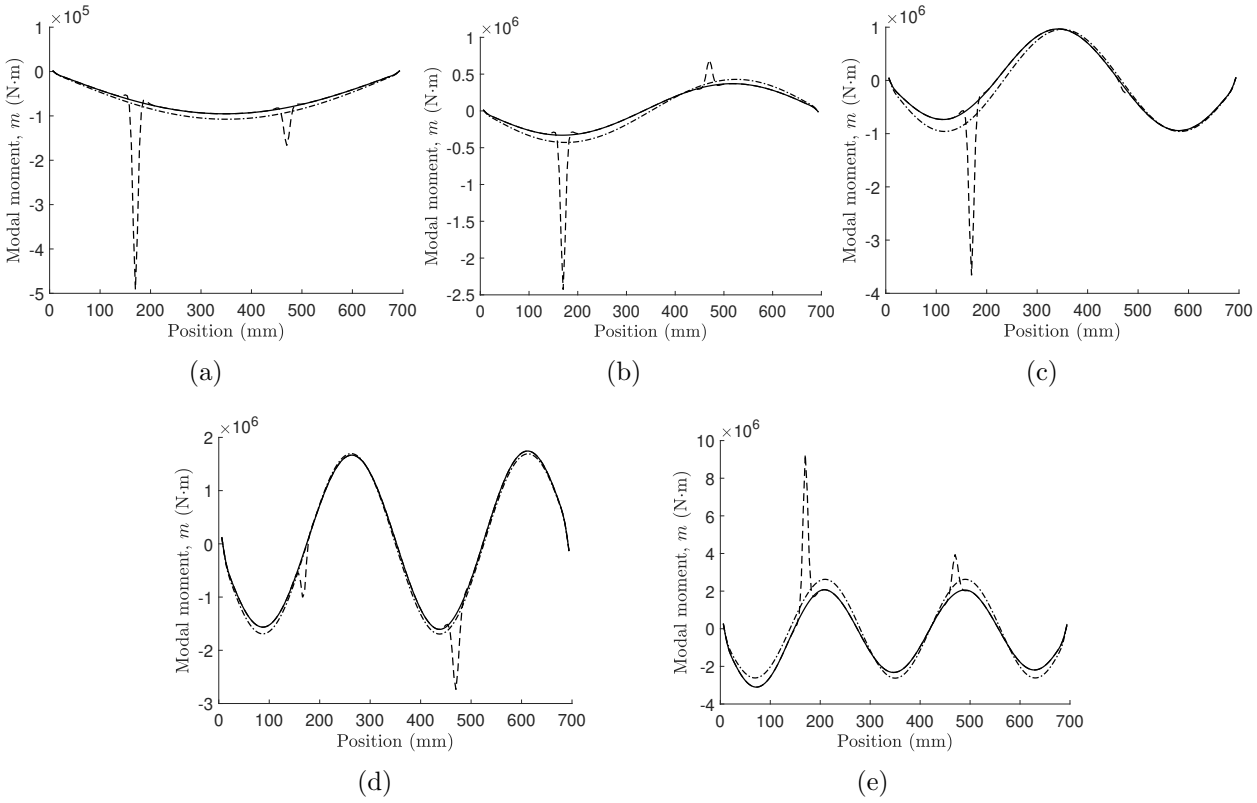


Figure 5: Estimated damaged modal bending moment ($m_{\mathrm{D}}$) of the example (Set-4) for (a) Mode 1, (b) Mode 2, (c) Mode 3, (d) Mode 4, (e) Mode 5 (dashed line represents a direct estimate of $m_{\mathrm{D}}$ from finite difference computation; solid line represents the spline fit of $m_{\mathrm{D}}$ and dash-dotted line represents $m_{\mathrm{R}}$).

Table 4: Undamaged ($m_{\mathrm{R}}$) and damaged ($m_{\mathrm{D}}$) bending moments ($N \cdot m$) at the damage locations of D1 and D2 for the Set-4 example.

| | Mode 1 | | Mode 2 | | Mode 3 | | Mode 4 | | Mode 5 | |
|---|---|---|---|---|---|---|---|---|---|---|
| | D1 | D2 | D1 | D2 | D1 | D2 | D1 | D2 | D1 | D2 |
| $m_{\mathrm{R}}$ | $-7.43e4$ | $-9.23e4$ | $-4.28e5$ | $3.77e5$ | $-7.21e5$ | $-4.15e4$ | $-1.42e5$ | $-1.42e6$ | $1.66e6$ | $2.36e6$ |
| $m_{\mathrm{D}}$ | $-6.67e4$ | $-8.13e4$ | $-3.30e5$ | $3.40e5$ | $-4.90e5$ | $-9.38e4$ | $-1.18e5$ | $-1.33e6$ | $1.13e6$ | $1.87e6$ |

By applying Eqs (7) and (8), one can get the DSI of D1 and D2 for each mode (Table 5). It can be seen that the DSI for both damage are consistent among the identified modes. However, when the damage is close to a node, the DSI exhibits a deviation, as it can be observed in Mode 3 at D2 and in Mode 4 at D1. Notwithstanding, the variance of the DSI of both damage shows that the DSI is not influenced by the mode order.

As described in the preceding section, the procedure for the final quantification of the damage in terms of relative severity is performed by comparing the obtained DSI with the values from a Reference Map. In this numerical example, the model used for the computation of the values of the Reference Map is the same as the one used for the simulation of the

Table 5: DSI of damage for the Set-4 example.

| Damage | Mode 1 | Mode 2 | Mode 3 | Mode 4 | Mode 5 | Variance |
|---|---|---|---|---|---|---|
| D1 | −29.3 | −29.2 | −29.2 | −28.7 | −29.2 | 0.057 |
| D2 | −32.0 | −32.0 | −32.4 | −32.0 | −31.9 | 0.038 |

numerical tests, but with only one single damage at location 350 mm. In order to illustrate the consistency and reliability of the Reference Map, reference values of the first 5 modes are obtained for three different boundary conditions: (1) simply-supported (SSB), (2) fixed-fixed (FFB), and (3) free-free (FREE). In addition, values from a static analysis with a point load at location 600 mm is also included. The independence of the proposed DSI with respect to the boundary conditions for the static cases (STC) has been already shown in Reference [1], so only one set of values is presented (they are obtained from the simply-supported situation). Figure 6 shows the obtained Reference Maps and there is a very good agreement among all of them, showing their independence from the definition of the boundary conditions, mode order and analysis type.

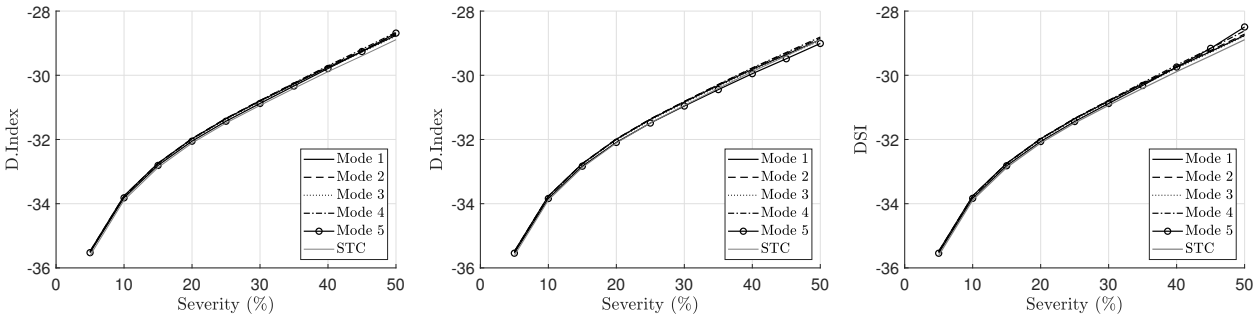


Figure 6: Reference Maps for the numerical illustration (Set-4) for the first five modes for: (a) simply-supported, (b) fixed-fixed, (c) free-free; and the simply-supported static case (STC).

By comparing the DSI values in Table 5 with the reference values from Figure 6, one gets the estimates of the depth of the two notches (Table 6). In general, all three Reference Maps of different mode shapes lead to accurate estimates of the notch depth and the static Reference Map results in similar quantification results, which confirms the validity of the proposed method. However, as expected, the estimated depths of D1 in Mode 4 and D2 in Mode 3 indicate that even in noise-free condition, the method exhibits difficulty in quantifying those damage close to a node.

### *3.2. Sparse grid (Set-20)*

A simulation for the 20 mm spacing between sensors (Set-20) is used for the analysis of a practical situation in which the number of sensors are limited. A major effect of a reduction in the number of measuring points when applying the wavelet transform, is that the wavelet function covers a longer span of the beam for each scale, thereby, limiting the practical

Table 6: Estimated damage depths (mm) of the Set-4 example.

| DSI Ref. | Mode 1 | | Mode 2 | | Mode 3 | | Mode 4 | | Mode 5 | |
|---|---|---|---|---|---|---|---|---|---|---|
| Map | D1 | D2 | D1 | D2 | D1 | D2 | D1 | D2 | D1 | D2 |
| SSB | 9.8 | 5.0 | 10.0 | 4.9 | 10.2 | 4.3 | 10.8 | 4.9 | 10.0 | 5.2 |
| FFB | 10.2 | 5.0 | 10.2 | 5.0 | 10.4 | 4.3 | 11.2 | 5.0 | 10.6 | 5.3 |
| FREE | 9.8 | 5.0 | 10.0 | 4.9 | 10.2 | 4.3 | 10.7 | 4.9 | 9.7 | 5.2 |
| STC | 10.2 | 5.2 | 10.3 | 5.2 | 10.3 | 4.5 | 11.2 | 5.2 | 10.3 | 5.3 |

number of scales to be used. In this numerical example, only three scales are used in order to avoid a combined effect of both damage on the wavelet coefficients. In addition, the wavelet coefficients at the damage location represent information of the signal in a less localized way, being affected by the shape of the incremental mode shapes over a longer region at both sides of the damage. This phenomenon is more significant when the incremental mode shape is more oscillatory and curvature changes are more significant, such as in higher order modes, beams with higher restrains at the supports or closely spaced damage, etc. In such situations, results are more sensitive to the experimental noise. Figure 7 shows the first five incremental mode shapes and the corresponding wavelet coefficients of Set-20.

As observed previously in the results of Set-4, due to the symmetry of the Gaus4 wavelet function, the wavelet coefficients exhibit two local extreme values one next to the other at the damage location. This alternation of the local extreme CWT values in the space domain may occur from one scale to another when the measuring grid is sparse, which means the DLI at the damage locations does not always equal the total number of scales (Figure 8). The DLI at the damage location together with the DLI at one of its adjacent locations, of the same sign, might sum up to the total number of scales, such as D1 in Mode 3, Mode 4 and Mode 5, and D2 in Mode 1, Mode 2 and Mode 3. In these cases, the damage locations can be well predicted by considering this phenomenon of spread adjacent local extreme values.

The presented results illustrate how the accuracy of the localization process is reduced by the reduction of the density of the measuring grid, especially for higher order modes. Table 7 shows the identified damage locations, which are in good agreement with the exact values.

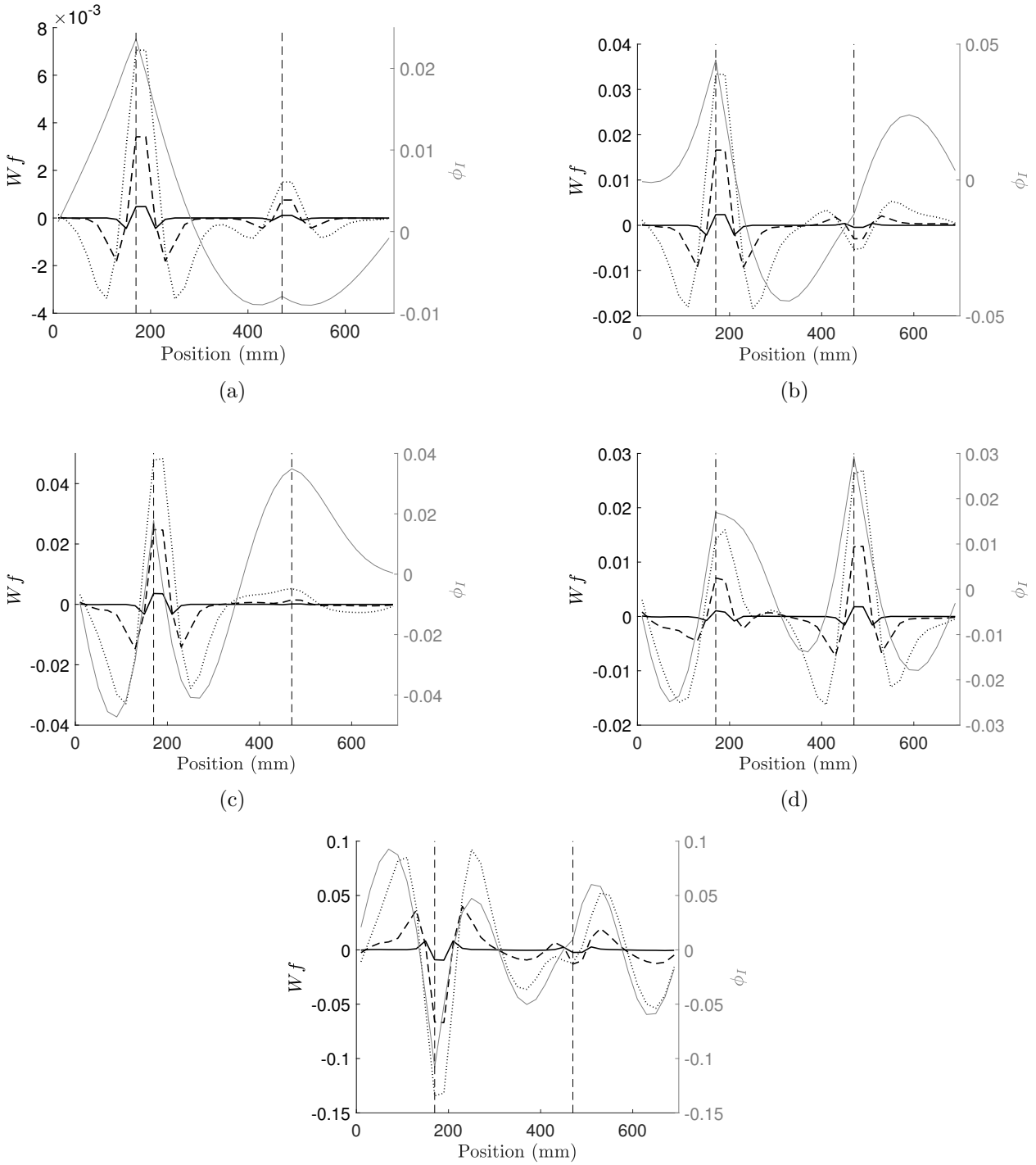


Figure 7: The incremental mode shapes (gray solid lines) and their wavelet coefficients (black lines) of the example (Set-20): (a) Mode 1, (b) Mode 2, (c) Mode 3, (d) Mode 4, (e) Mode 5 (Scale 1: solid lines; Scale 2: dashed lines; Scale 3: dotted lines; the vertical dashed lines mark the damage locations).

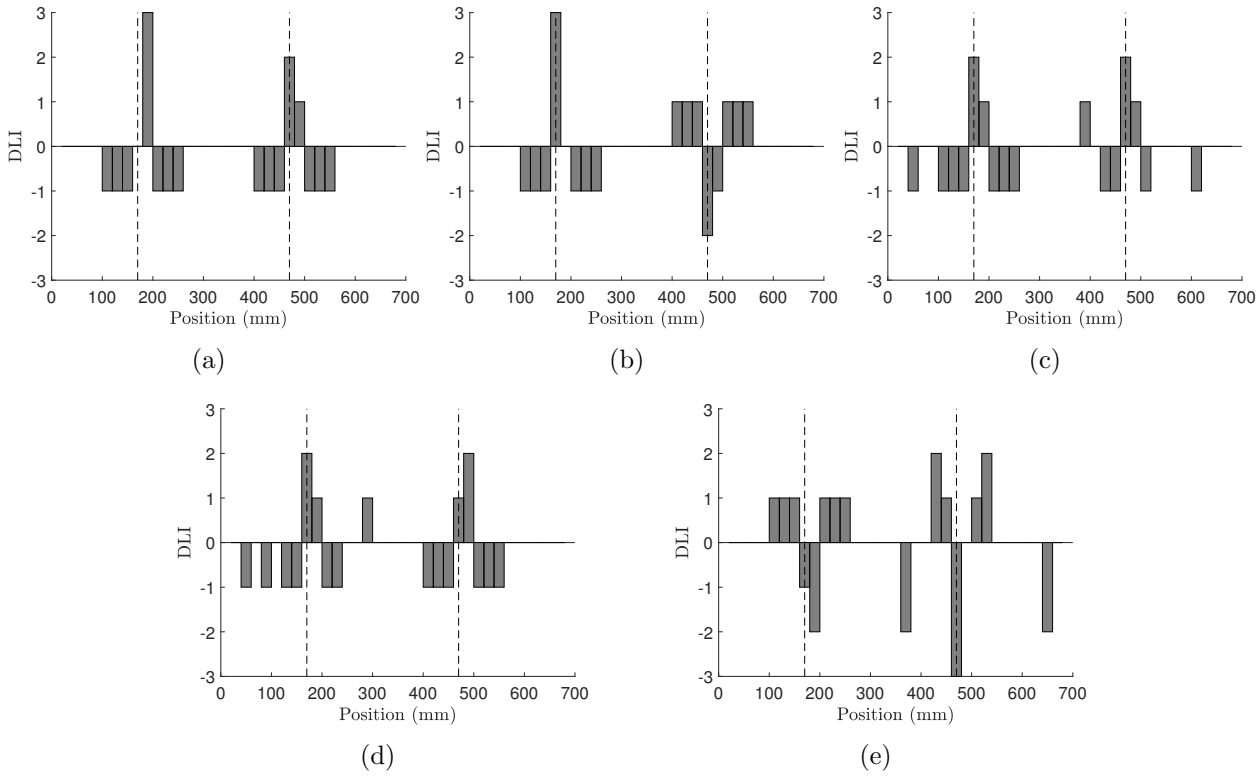


Figure 8: The DLI of each mode of the example (Set-20): (a) Mode 1, (b) Mode 2, (c) Mode 3, (d) Mode 4, (e) Mode 5 (Scale 1: solid lines; Scale 2: dashed lines; Scale 3: dashed-dotted lines; Scale 4: dotted lines; the vertical dashed lines mark the damage locations).

Table 7: Predicted damage locations (mm) of the Set-20 example.

| Damage | Mode 1 | Mode 2 | Mode 3 | Mode 4 | Mode 5 |
|---|---|---|---|---|---|
| D1 | 190 | 170 | 170 | 170 | 190 |
| D2 | 470 | 470 | 470 | 490 | 470 |

The values of the DSI for both damage are included in Table 8. By comparing the values with those from Table 5, obtained for Set-4, one notes that the DSI values are affected by the number of measuring points. In addition, it can be seen that the consistency between the different modes for each damage (illustrated by the variance included in Table 5 and 8) is reduced when less number of measuring points are used for the identification.

Table 8: DSI of the damage of the Set-20 example.

| Damage | Mode 1 | Mode 2 | Mode 3 | Mode 4 | Mode 5 | Variance |
|---|---|---|---|---|---|---|
| D1 | $-26.0$ | $-25.9$ | $-25.8$ | $-25.4$ | $-26.3$ | 0.115 |
| D2 | $-28.4$ | $-28.2$ | $-28.9$ | $-27.7$ | $-29.5$ | 0.473 |

By following the same procedure explained in the previous section, the Reference Maps from modal analysis (three different boundary conditions) and static analysis (simply-supported) are established (Figure 9). It must be recalled that the Reference Map must be obtained with the same number of measuring points from the tests, as the value of the DSI is affected by this number. By comparing Figure 9 with Figure 6, it can be clearly seen that the consistency of the Reference Maps are less for Set-20 than for Set-4, especially for Mode 4 and Mode 5. As explained before, as more oscillation takes place in the signal, the accuracy of the wavelet transform is more affected by the reduction of the measuring points.

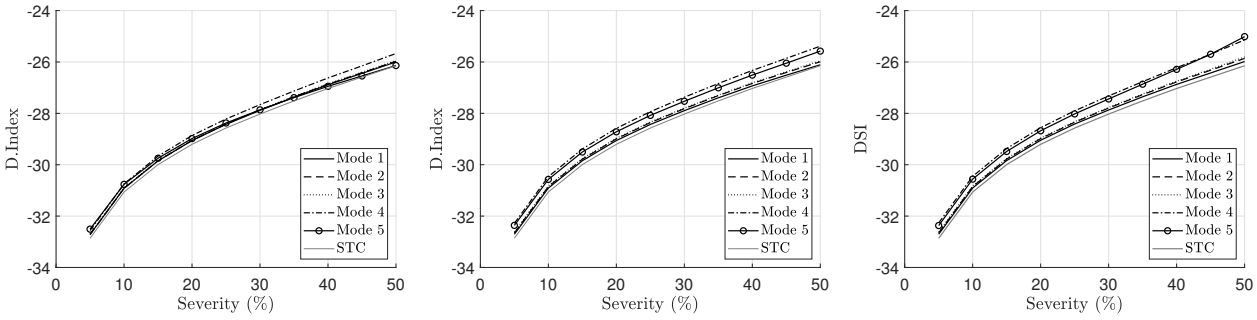


Figure 9: The DSI reference maps for different boundary conditions (Set-20): (a) simply-supported, (b) fixed-fixed, (c) free-free.

The estimated notch depths using Set-20 are presented in Table 9. The estimates from Mode 1, Mode 2, and Mode 3 are better than those from Mode 4 and Mode 5 because of the more significant effect of the reduction in the spatial resolution for higher order modes. Similar to Set-4, at cases where damage is close to a node, the estimate becomes less accurate than others. In general, the estimates of Set-20 are less accurate than those of Set-4. However, considering the sparsity of the data, the damage identification should be considered successful.

Table 9: Estimated damage depths (mm) of the Set 2 example.

| DSI Ref. | Mode 1 | | Mode 2 | | Mode 3 | | Mode 4 | | Mode 5 | |
|---|---|---|---|---|---|---|---|---|---|---|
| Map | D1 | D2 | D1 | D2 | D1 | D2 | D1 | D2 | D1 | D2 |
| SSB | 9.7 | 5.0 | 10.2 | 5.4 | 10.2 | 4.2 | 10.6 | 6.0 | 9.5 | 3.3 |
| FFB | 10.0 | 5.0 | 10.3 | 5.3 | 10.4 | 4.1 | 10.0 | 5.4 | 8.4 | 3.0 |
| FREE | 9.7 | 5.0 | 10.0 | 5.2 | 10.0 | 4.1 | 9.5 | 5.3 | 8 | 3.0 |
| STC | 10.0 | 5.3 | 10.5 | 5.7 | 10.7 | 4.5 | 11.8 | 6.6 | 9.6 | 3.6 |

### *3.3. Discussion of theoretical and practical issues*

Through the presented numerical example, it has been shown that the DSI is not dependent on the damage location, boundary conditions, mode order, and analysis type static or dynamic), given sufficient measurement points. The consistency between the different curves of

the presented Reference Maps for higher number of measuring points (Set-4) demonstrates the theoretical independency of the DSI from boundary conditions and mode order. On the other hand, the accuracy of the predicted damage severities obtained for different damage positions (that do not correspond to the position used for the Reference Maps) demonstrate the independency of the DSI from the damage location. By analyzing the results for cases Set-4 and Set-20, it is illustrated how the accuracy is affected by the sampling interval. When the measurement points are limited, the proposed DSI is more affected by the effect of different boundary conditions, mode order and damage location. As a result, it performs better for low order modes as the number of measuring points is smaller.

The boundary conditions used to build the Reference Map do not theoretically require to be consistent with the real situation since the effect of the damage is locally analyzed at the damage location. This is a practical advantage because of the uncertainty about the actual behavior of the boundary conditions in real applications. However, a reduced number of measuring points may affect the independence of the DSI with respect to the boundary conditions as well as the damage location. In such situations, the accuracy of the identification procedure can be reduced by this influence, as it illustrated by the results from the Set-20 configuration.

Regarding the sensitivity of the proposed methodology, it must be noted that, in noise-free conditions, any little damage could be accurately identified as long as a big enough number of measuring points is considered. The presented numerical illustration shows how the accuracy and sensitivity of the damage identification is affected by the number of measuring points. For this reason, in practical applications, an estimation of the smallest damage that can be be detected can be performed through a specific numerical sensitivity analysis considering the actual number of measuring points and the experimentally available and reliable mode shapes.

## 4. Experimental case study

### *4.1. Modal tests*

A steel beam of the same dimensions of that from the numerical model (length 700 mm, width 80 mm, and height 20 mm) is used to examine the proposed method. The beam is simply-supported at two ends (Figure 10 (a)). Mode shapes were identified by performing traditional impact tests. A total of 35 positions were labeled on the beam as P1 (the left support), P2, ..., P35 (the right support) with an equal 20 mm spacing (Figure 11). A set of 33 magnetic disks were used to connect the beam and the piezoelectric accelerometers. A total of 17 accelerometers, all with nominal sensibility of 100 mV/g were divided into two setups in order to maximize the number of measurements (33 in total). One sensor was fixed at the impact location (P10) serving as the reference sensor (Figure 10 (b)). The rest of the accelerometers were used as roving sensors. Setup 1 consists of even positions and Setup 2 consists of odd positions, from P2 to P34. Two artificial notches, as shown in Figure 10 (c), were introduced as damage at locations 170 mm and 470 mm.

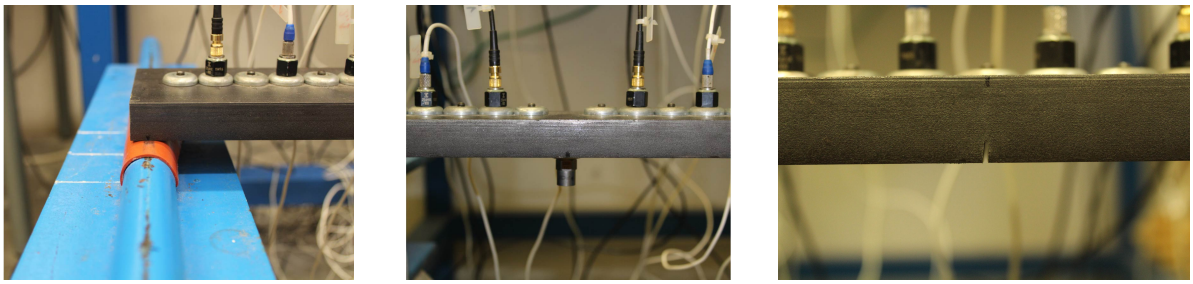

(a) (b) (c)

Figure 10: The configuration of the impact test (a) the boundary condition; (b) sensors around the impact position; (c) damage of 5 mm.

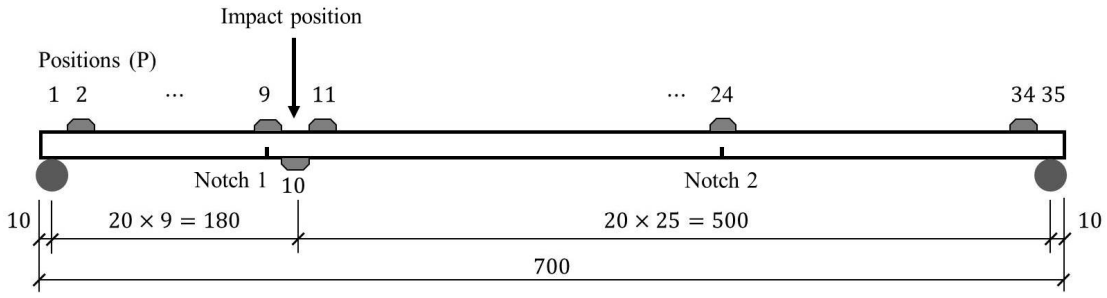


Figure 11: The configuration of the positions on the test beam (unit: mm).

For the modal identification, the impact excitation was introduced by an impact hammer of 11 mV/N sensitivity. The averaged Frequency Response Functions (FRF) were obtained from 10 impacts for each setup and the mass-normalized mode shapes were identified. The identified mode shapes for the Reference State are shown in Figure 12. They form the reference information for the subsequent damage identification process. Figure 12 shows that the response at the supports does not correspond to an ideal simply supported-beam. In addition, it can be seen that none of the two damage are situated at any node location of any of the identified modes. In addition, Figure 12 shows that different modes have distinct levels of experimental noise. The presence of noise in the mode shapes definitely contaminates the damage identification results. As a result, noisy mode shapes should be disregarded and only reliable modes should be kept for the analysis.

In this paper, a procedure based on noise evaluation is proposed for selecting the most suitable mode shapes. In order to quantify and compare the relative noise pollution of different modes, the noise level is characterized through a normalized standard deviation index, $\eta_j$ (Eqs. (9) and (10)):

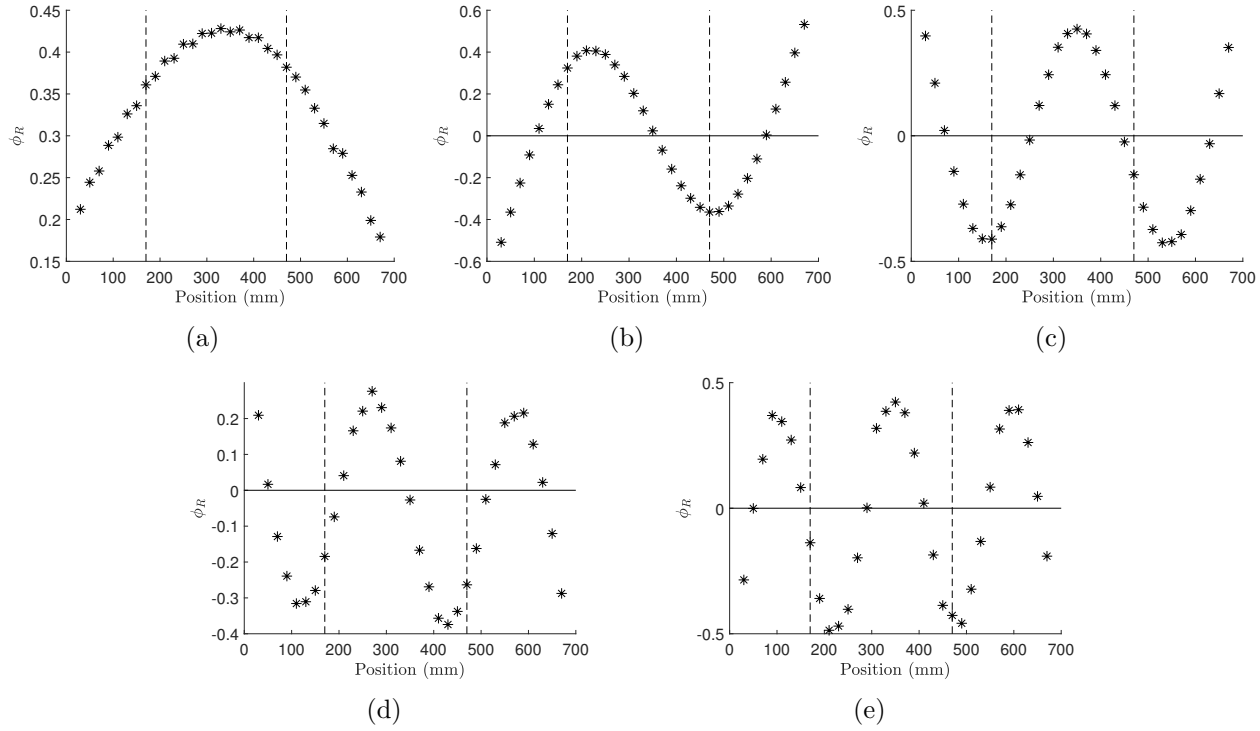


Figure 12: The first 5 reference mode shapes of the test beam ($\phi_{\mathrm{R}}$): (a) Mode 1, (b) Mode 2, (c) Mode 3, (d) Mode 4, (e) Mode 5 (the vertical dashed lines mark the damage locations).

$$\eta_j = \frac{\tilde{\sigma}_j}{\max(\phi_j) - \min(\phi_j)}, \qquad j = 1, 2, 3, 4, 5 \tag{9}$$

$$\tilde{\sigma}_j = \sqrt{\frac{1}{N-1}\sum_{i=1}^{N}(\phi_{i,j} - \bar{\phi}_{i,j})^2}, \quad i = 1, 2, \cdots, N \tag{10}$$

where $\phi_{i,j}$ is the $i$th measurement of the $j$th experimental mode shape $\phi_j$, $\bar{\phi}_{i,j}$ is the spline fit of the mode shape, served here as noise-free reference for noise quantification, and $N$ is the number of measurements. The normalized standard deviation indices for each mode are included in Table 10. They show that Mode 2 and Mode 3 are significantly less affected by noise than the rest of the identified modes. Therefore, in order to reduce the effect of experimental noise in the final results, only Mode 2 and Mode 3 are considered for the application of the proposed damage detection methodology.

This paper proposes the application of the presented mode selection criterion in practical applications. However, the definition of a threshold value for the normalized standard deviation index and subsequently the number of modes to be selected will depend on the quality of the experimental data. A specific analysis is necessary for each application.

Table 10: The noise level of the identified modes.

| | Mode 1 | Mode 2 | Mode 3 | Mode 4 | Mode 5 |
|---|---|---|---|---|---|
| $\eta$ | 0.011 | 0.0012 | 0.0032 | 0.0092 | 0.0145 |

*4.2. Damage identification*

Two damage scenarios of double damage are investigated. In Scenario 1 (S1), the two notches are both of 5 mm (25% severity), and, in Scenario 2 (S2), the two notches are both of 10 mm (50% severity) at the same locations. Figure 13 shows the damaged mode shapes of Mode 2 and Mode 3 for the two damage scenarios. It can be seen that both mode shapes are well identified and the noise level is low. The damaged mode shapes are similar to the undamaged ones, which means that the influence of damage is not perceptible from visual inspection.

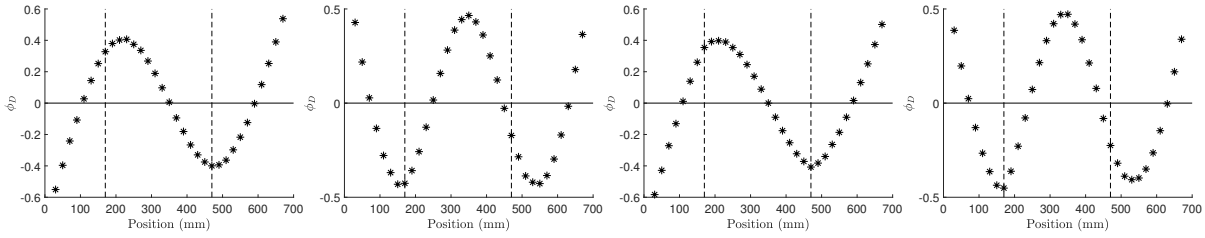


Figure 13: The damaged mode shapes of the test beam ($\phi_{\mathrm{D}}$): (a) S1 Mode 2; (b) S1 Mode 3; (c) S2 Mode 2; (d) S2 Mode 3 (the vertical dashed lines mark the damage locations).

By taking the difference of the damaged and undamaged mode shapes, the experimental noise effect becomes discernible (Figure 14). Therefore, the mode shapes, $\phi_{\mathrm{R}}$ and $\phi_{\mathrm{D}}$, are fitted by splines to diminish the noise effect. The smoothed incremental mode shapes, $\bar{\phi}_{\mathrm{I}}$, are obtained by subtracting $\bar{\phi}_{\mathrm{R}}$ from $\bar{\phi}_{\mathrm{D}}$, with $\bar{\phi}_{\mathrm{R}}$ and $\bar{\phi}_{\mathrm{D}}$ being the fitted undamaged and damaged mode shapes, respectively. Figure 14 shows that the curve-fitting process reduces significantly the noise pollution and preserves the damage induced discontinuities.

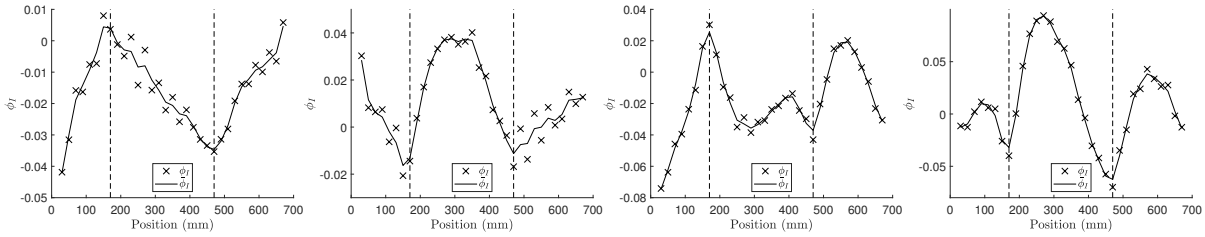


Figure 14: The incremental damaged mode shapes of the test beam ($\phi_{\mathrm{I}}$) and their smoothing spline fits ($\bar{\phi}_{\mathrm{I}}$): (a) S1 Mode 2; (b) S1 Mode 3; (c) S2 Mode 2; (d) S2 Mode 3 (the vertical dashed lines mark the damage locations).

The wavelet analysis is applied to the fitted incremental mode shapes $\bar{\phi}_{\mathrm{I}}$. Due to the limited number of sensors, only 3 scales are used. The wavelet coefficients are shown in Figure 15 and the corresponding DLI obtained by applying Eqs. (4) and (5) are shown in Figure 16. The potential damage locations shown in Table 11 are identified using the criteria established in the numerical example. Both D1 and D2 are identified successfully in all cases. For S1 (25% damage), several false positive damage locations are predicted, while for S2 (50% damage), no false positive locations are identified. Since the false positives can be due to specific reasons for each mode, and, therefore, might not be consistent among them, it is proposed to use the benefit of having several identified modes by computing a Combined DLI (CDLI) of all the modes, so that the number of false positives can be reduced. This combination can be carried out by adding up the absolute values of DLI of each mode $j$ at each location $i$ (Eq. (11)):

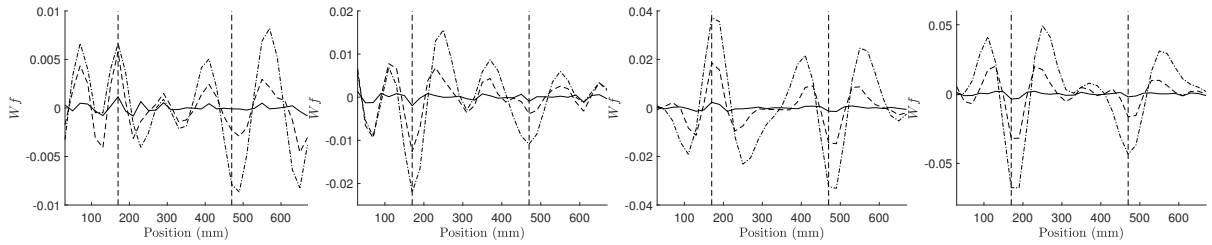


Figure 15: The wavelet coefficients of the fitted incremental mode shapes (Scale 1: solid line; Scale 2: dashed line; Scale 3: dotted line; Scale 4: dash-dotted line): (a) S1 Mode 2; (b) S1 Mode 3; (c) S2 Mode 2; (d) S2 Mode 3 (the vertical dashed lines mark the damage locations).

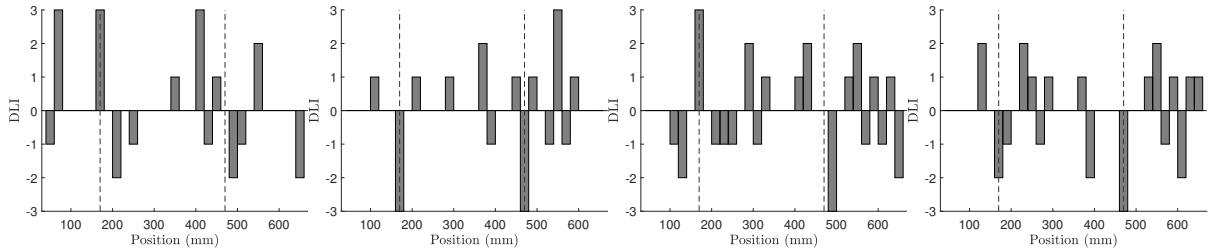


Figure 16: The Damage Locating Index (DLI) of (a) S1 Mode 2; (b) S1 Mode 3; (c) S2 Mode 2; (d) S2 Mode 3 (the vertical dashed lines mark the damage locations).

$$\mathrm{CDLI}_i = \sum_j |\mathrm{DLI}_{i,j}|, \quad j = 2, 3 \tag{11}$$

As shown in Figure 16, the absolute value of the DLI at the damage location is either 3 (the maximum number of scales) with no DLI of the same sign at its adjacent locations, or 2

Table 11: Potential damage locations of the experimental case study.

| Damage Scenario | Mode | Damage locations (mm) |
|---|---|---|
| 1 | 2 | 70, 170, 410, 490 |
| | 3 | 170, 470, 550 |
| 2 | 2 | 170, 490 |
| | 3 | 170, 470 |

with one of the two adjacent points having a DLI of value 1 of the same sign. Therefore, the potential damage is determined at locations with a $\text{CDLI}_i$ equaled or greater than 5. Figure 17 shows the obtained CDLI. it must be recalled that wavelet extreme values may appear at adjacent locations for different scales and modes, as it happens for D2 in both scenarios, S1 and S2. Hence, locations next to each other with both CDLI equaling 3 should also be considered damage location predictions. As a result, the predicted damage locations are 170 mm, 470 mm, and 550 mm for S1, and are 170 mm and 470 mm for S2.

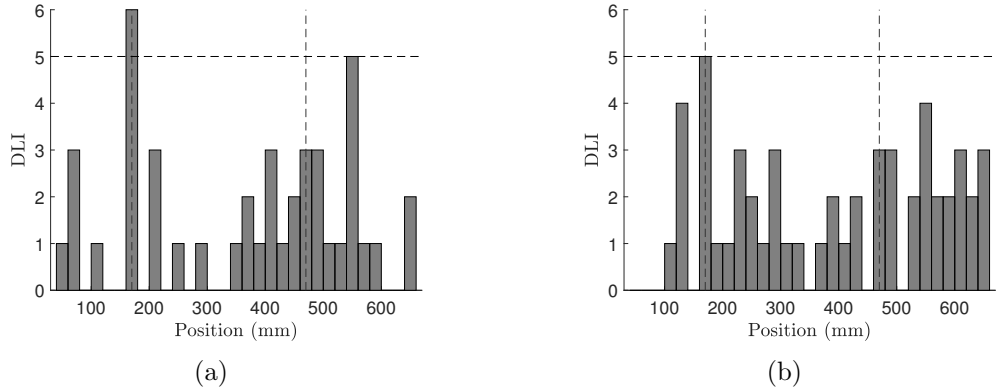


Figure 17: The Combined Damage Locating Index (CDLI) of (a) S1; (b) S2 (the vertical dashed lines mark the damage locations; the horizontal dashed line marks the threshold for potential damage locations).

Once the damage locations are identified, the modal damaged bending moment has to be identified at those locations from the estimation of the damaged modal curvature, as presented in the numerical illustration. In order to reduce the instability in the curvature estimates, a polynomial fit is applied. The order of the polynomial can be selected by checking the accuracy of the approach. When using real experimental noisy mode shapes instead of numerical ones, the polynomial fit is preferred rather than the spline fit. The reason is that the polynomial tends to approach smoothly the global trend whereas the spline fit keep partially the noisy irregularity, leading to higher instability in the curvature estimation. Moreover, the polynomial fit allows the analytical evaluation of the curvatures and no numerical differentiation is required. Figure 18 shows the polynomial fits of the experimental damaged mode shapes.

From the estimates of the modal bending moment at the predicted damage locations, the normalized wavelet coefficients and the DSI can be obtained. Since the boundary conditions

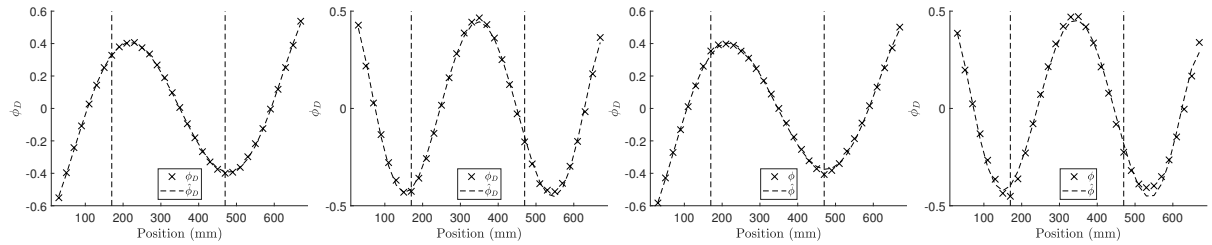


Figure 18: The damaged mode shapes of the test beam ($\phi_{\mathrm{D}}$) and their polynomial fits ($\hat{\phi}_{\mathrm{D}}$): (a) S1 Mode 2; (b) S1 Mode 3; (c) S2 Mode 2; (d) S2 Mode 3 (the vertical dashed lines mark the damage locations).

of the actual structure is none of the three perfect types applied in the numerical models, and the sparsity of the measurements makes that the DSI might be affected by the definition of the boundary conditions, it is recommended to use DSI Reference Maps of different boundary types for the severity assessment. The estimated notch depths using the DSI Reference Maps from Figure 9 are shown in Figure 19. In S1, both of the damage are underestimated from Mode 2, and D1 is overestimated while D2 is underestimated from Mode 3. The absolute error for the estimate of D1 is between $-1.5\,\mathrm{mm}$ and $1.5\,\mathrm{mm}$, and it is between $-1.2\,\mathrm{mm}$ and $-0.8\,\mathrm{mm}$ for D2. In S2, both Mode 2 and Mode 3 underestimate both damage. The prediction error for D1 is from $-2\,\mathrm{mm}$ to $-0.5\,\mathrm{mm}$, and for D2 is from $-3.0\,\mathrm{mm}$ to $-0.5\,\mathrm{mm}$.

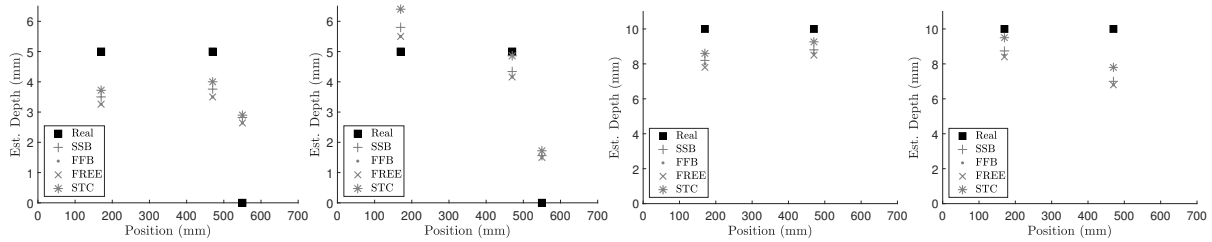


Figure 19: The estimated damage depth from Reference Maps of simply-supported (SSB), fixed-fixed (FFB), free-free (FREE) modal analysis and static (STC) analysis: (a) S1 Mode 2; (b) S1 Mode 3; (c) S2 Mode 2; (d) S2 Mode 3.

The experimental results show that the proposed method can successfully identified the locations of a double-damage situation, and estimate the severity to a certain accuracy level. However, with the conditions of the test, e.g. the number of measurements and the use of two sensor setups, the experimental case study serves as an illustration of the practical limits for the application of the proposed methodology.

## 5. Conclusions and remarks

In this paper, a damage identification method based on the use of CWT of mode shapes is presented. The damage is located by a Damage Locating Index, the counts of the local extreme wavelet coefficients for different scales. The damage severity can be further estimated by a Damage Severity Index using reference values based on numerical models. Through numerical illustrations, relevant issues of the application of the proposed method are studied, such as the influence of the number of measuring points, the use of different modes, the influence of uncertainty in the behavior of the boundary conditions, and the scale selection for wavelet analysis. It is shown that, when given sufficient measurements, the proposed DSI is applicable for both modal and static displacements, for beams with different boundary conditions, and for mode shapes of different orders.

A practical situation of limited sensors is considered and the numerical study of a beam with two damage shows that the proposed DLI and DSI can provide promising estimates on both the damage locations and severity. In addition, the experimental study shows that, with appropriate noise reducing tools, the proposed DLI can locate damage with high accuracy, and there is a tendency to underestimate the damage severity with the DSI. Questions regarding the exploitation of multiple modal displacements are yet to be studied. The experimental predictions do not exhibit a clear tendency among different modes for the same damage. As illustrated in this study, when using a higher number of measuring points and by reducing the experimental noise, the damage severity can be estimated with more accuracy.

In this study, the width of the notch damage is 1 mm in both the simulation and the real beam. It is, however, improbable in practice that the damage geometry type is a prior-knowledge. Future developments of the present study will include a sensitivity analysis of the proposed DSI to different parameters, such as the opening width of the notch and other damage types.

## Acknowledgments

The authors would like to acknowledge the financial support provided by the Spanish Ministries of Economy and Competitiveness, Science and Innovation under research project PID2019-109622RB-C21.

## References

[1] Q. Ma, M. Solís, P. Galvín, Wavelet analysis of static deflections for multiple damage identification in beams, Mechanical Systems and Signal Processing 147 (2021) 107103. doi:10.1016/j.ymssp.2020.107103.

[2] M. Solís, M. Algaba, P. Galvín, Continuous wavelet analysis of mode shapes differences for damage detection, Mechanical Systems and Signal Processing 40 (2) (2013) 645–666. doi:10.1016/j.ymssp.2013.06.006.

[3] M. S. Cao, W. Xu, W. X. Ren, W. Ostachowicz, G. G. Sha, L. X. Pan, A concept of complex-wavelet modal curvature for detecting multiple cracks in beams under noisy conditions, Mechanical Systems and Signal Processing 76-77 (2016) 555–575. doi:10.1016/j.ymssp.2016.01.012.

[4] R. Janeliukstis, S. Rucevskis, M. Wesolowski, A. Chate, Experimental structural damage localization in beam structure using spatial continuous wavelet transform and mode shape curvature methods, Measurement: Journal of the International Measurement Confederation 102 (2017) 253–270. doi:10.1016/j.measurement.2017.02.005.

[5] V. Shahsavari, L. Chouinard, J. Bastien, Wavelet-based analysis of mode shapes for statistical detection and localization of damage in beams using likelihood ratio test, Engineering Structures 132 (2017) 494–507. doi:10.1016/j.engstruct.2016.11.056.

[6] A. Ghanbari Mardasi, N. Wu, C. Wu, Experimental study on the crack detection with optimized spatial wavelet analysis and windowing, Mechanical Systems and Signal Processing 104 (2018) 619–630. doi:10.1016/j.ymssp.2017.11.039.

[7] A. Deng, M. Cao, Q. Lu, W. Xu, Identification of multiple cracks in composite laminated beams using perturbation to dynamic equilibrium, Sensors 21 (18) (2021). doi:10.3390/s21186171.

[8] R. Kumar, S. K. Singh, Crack detection near the ends of a beam using wavelet transform and high resolution beam deflection measurement, European Journal of Mechanics, A/Solids 88 (January) (2021) 104259. doi:10.1016/j.euromechsol.2021.104259.

[9] U. Andreaus, P. Baragatti, P. Casini, D. Iacoviello, Experimental damage evaluation of open and fatigue cracks of multi-cracked beams by using wavelet transform of static response via image analysis, Structural Control and Health Monitoring 24 (4) (2017) 1–16. doi:10.1002/stc.1902.

[10] L. F. Zhu, L. L. Ke, X. Q. Zhu, Y. Xiang, Y. S. Wang, Crack identification of functionally graded beams using continuous wavelet transform, Composite Structures 210 (November 2018) (2019) 473–485. doi:10.1016/j.compstruct.2018.11.042.

[11] Y. Xu, D.-M. Chen, W. Zhu, Modal parameter estimation using free response measured by a continuously scanning laser Doppler vibrometer system with application to structural damage identification, Journal of Sound and Vibration 485 (2020) 115536. doi:10.1016/J.JSV.2020.115536.

[12] J. Baqersad, P. Poozesh, C. Niezrecki, P. Avitabile, Photogrammetry and optical methods in structural dynamics – A review, Mechanical Systems and Signal Processing 86 (2017) 17–34. doi:10.1016/j.ymssp.2016.02.011.

[13] R. Nigam, S. K. Singh, Crack detection in a beam using wavelet transform and photographic measurements, Structures 25 (March) (2020) 436–447. doi:10.1016/j.istruc.2020.03.010.

[14] A. Katunin, J. V. Araújo dos Santos, H. Lopes, Damage identification by wavelet analysis of modal rotation differences, Structures 30 (October 2020) (2021) 1–10. doi:10.1016/j.istruc.2021.01.010.

[15] H. Jahangir, H. Hasani, M. R. Esfahani, Wavelet-based damage localization and severity estimation of experimental RC beams subjected to gradual static bending tests, Structures 34 (September) (2021) 3055–3069. doi:10.1016/j.istruc.2021.09.059.

[16] E. Douka, S. Loutridis, A. Trochidis, Crack identification in beams using wavelet analysis, International Journal of Solids and Structures 40 (13-14) (2003) 3557–3569. doi:10.1016/S0020-7683(03)00147-1.

[17] S. Loutridis, E. Douka, A. Trochidis, Crack identification in double-cracked beams using wavelet analysis, Journal of Sound and Vibration 277 (4-5) (2004) 1025–1039. doi:10.1016/j.jsv.2003.09.035.

[18] L. Montanari, A. Spagnoli, B. Basu, B. Broderick, On the effect of spatial sampling in damage detection of cracked beams by continuous wavelet transform, Journal of Sound and Vibration 345 (2015) 233–249. doi:10.1016/j.jsv.2015.01.048.

[19] M. Mininni, S. Gabriele, H. Lopes, J. V. Araújo dos Santos, Damage identification in beams using speckle shearography and an optimal spatial sampling, Mechanical Systems and Signal Processing 79 (2016) 47–64. doi:10.1016/j.ymssp.2016.02.039.

[20] L. Pedroso, A. Arco, I. Figueiras, J. V. Araújo dos Santos, J. L. Fernandes, H. Lopes, Application of cubic spline interpolation with optimal spatial sampling for damage identification, Structural Control and Health Monitoring 29 (1) (2022) 1–24. doi:10.1002/stc.2856.

[21] Q. Ma, M. Solís, Application of wavelet analysis for crack localization and quantification in beams using static deflections, in: Proceedings of the 13th International Conference on Damage Assessment of Structures, Springer, Singapore, 2020, pp. 135–149. doi:10.1007/978-981-13-8331-1_10.

[22] Q. Ma, M. Solis, Damage localization and quantification in beams from slope discontinuities in static deflections, Smart structures and systems 22 (3) (2018) 291–302.

[23] Q. Ma, M. Solís, Multiple damage identification in beams from full-field digital photogrammetry, Journal of Engineering Mechanics 145 (8) (2019) 1–12. doi:10.1061/(ASCE)EM.1943-7889.0001629.

[24] A. Gentile, A. Messina, On the continuous wavelet transforms applied to discrete vibrational data for detecting open cracks in damaged beams, International Journal of Solids and Structures 40 (2) (2003) 295–315. doi:10.1016/S0020-7683(02)00548-6.

[25] M. Rucka, K. Wilde, Application of continuous wavelet transform in vibration based damage detection method for beams and plates, Journal of Sound and Vibration 297 (2006) 536–550. doi:10.1016/j.jsv.2006.04.015.

[26] Selection of suitable mother wavelet along with vanishing moment for the effective detection of crack in a beam, Mechanical Systems and Signal Processing 163 (May 2021) (2022) 108136. doi:10.1016/j.ymssp.2021.108136.

[27] A. Messina, Refinements of damage detection methods based on wavelet analysis of dynamical shapes, International Journal of Solids and Structures 45 (14-15) (2008) 4068–4097. doi:10.1016/j.ijsolstr.2008.02.015.

[28] L. Montanari, B. Basu, A. Spagnoli, B. M. Broderick, A padding method to reduce edge effects for enhanced damage identification using wavelet analysis, Mechanical Systems and Signal Processing 52-53 (1) (2015) 264–277. doi:10.1016/j.ymssp.2014.06.014.

[29] J. C. Hong, Y. Y. Kim, H. C. Lee, Y. W. Lee, Damage detection using the Lipschitz exponent estimated by the wavelet transform: Applications to vibration modes of a beam, International Journal of Solids and Structures 39 (7) (2002) 1803–1816. doi:10.1016/S0020-7683(01)00279-7.